J Comput Neurosci
DOI 10.1007/s10827-009-0169-z

A large-scale model of the locust antennal lobe

Mainak Patel · Aaditya V. Rangan · David Cai

Received: 26 September 2008 / Revised: 11 March 2009 / Accepted: 2 June 2009

Abstract The antennal lobe (AL) is the primary structure within the locust's brain that receives information from olfactory receptor neurons (ORNs) within the antennae. Different odors activate distinct subsets of ORNs, implying that neuronal signals at the level of the antennae encode odors combinatorially. Within the AL, however, different odors produce signals with long-lasting dynamic transients carried by overlapping neural ensembles, suggesting a more complex coding scheme. In this work we use a large-scale point neuron model of the locust AL to investigate this shift in stimulus encoding and potential consequences for odor discrimination. Consistent with experiment, our model produces stimulus-sensitive, dynamically evolving populations of active AL neurons. Our model relies critically on the persistence time-scale associated with ORN input to the AL, sparse connectivity among projection neurons, and a synaptic slow inhibitory mechanism. Collectively, these architectural features can generate network odor representations of considerably higher dimension than would be generated by a direct feed-forward representation of stimulus space.

Keywords Linear discriminability · Principal component analysis

Action Editor: T. Sejnowski

Electronic supplementary material The online version of this article (doi:10.1007/s10827-009-0169-z) contains supplementary material, which is available to authorized users.

M. Patel
The Sackler Institute of Graduate Biomedical Sciences,
NYU School of Medicine,
550 First Avenue,
New York, NY 10016, USA
e-mail: Mainak.Patel@med.nyu.edu

A. V. Rangan (✉) · D. Cai
Courant Institute of Mathematical Sciences, New York University,
251 Mercer Street,
New York, NY 10012-1185, USA
e-mail: Rangan@cims.nyu.edu

D. Cai
e-mail: Cai@cims.nyu.edu

1 Introduction

Olfaction is the most primitive of the senses; in fact, it is the only sensory pathway that does not relay in the thalamus prior to synapsing in a sensory processing area (Costanzo and Morrison 1989; Moulton 1974; Graziadei and Metcalf 1971). Accordingly, early olfactory processing is well-conserved across species in the sense that primary olfactory structures in a wide range of species, from insects to mammals, seem to share certain key anatomical and functional properties. Such properties include the combinatorial representation of an odor stimulus at the olfactory receptor neuron (ORN) level and the glomerular organization of the primary sensory structure receiving ORN input (Hildebrand and Shepherd 1997). In mammals, the olfactory bulb (OB) receives primary ORN input, while the insect analogue of the OB is the antennal lobe (AL).

The locust AL consists of inhibitory local neurons (LNs) and excitatory projection neurons (PNs), the latter of which comprise the sole output cells of the AL and project to the multimodal mushroom body (Heisenberg 1998; Strausfeld et al. 1998). The AL is organized anatomically into bundles of cells and fibers termed glomeruli, each of which receives convergent input from ORNs expressing the same olfactory receptor (Vosshall et al. 2000; Treloar et al. 2002; Gao et al.

Published online: 23 June 2009

2000; Axel 1995). Upon presentation of an odor, a specific subset of ORNs is stimulated and the corresponding AL glomeruli receive ORN input. Within a few hundred milliseconds, however, the set of active PNs decorrelates from the set of stimulated glomeruli, and throughout the first second of stimulus presentation the set of active PNs evolves dynamically in a stimulus-specific manner. Within 1 s, the set of active PNs ceases to evolve and the network reaches a fixed point; the network remains at this fixed point until stimulus offset, after which the set of active PNs again evolves transiently prior to returning to baseline firing rates within the next several seconds (Mazor and Laurent 2005). This large-scale network behavior is reflected in single cell activity via the phenomenon of slow temporal patterning—the firing rate of each PN in response to a stimulus exhibits a reproducible, odor-specific temporal structure; this temporal structure varies from PN to PN for a given odor and for a single PN across different odors (Laurent et al. 1996). Additionally, PN activity is synchronized in an odor response, as evidenced by the emergence of strong 20 Hz oscillations in the local field potential (LFP) of the AL shortly after stimulus presentation (Laurent and Davidowitz 1994).

Thus, the AL transforms the neural representation of an odor stimulus from a combinatorial code to a dynamic code—the ORNs represent an odor by a specific subset of active receptor cells, while the AL redistributes this glomerular input pattern across the entire PN network and represents the odor as dynamically evolving subsets of active PNs (Laurent et al. 2001). Since there is no evidence that the AL receives feedback from higher structures, this transformation of the odor representation can be understood entirely in terms of stimulus encoding. As seen in the zebrafish OB (Friedrich and Laurent 2001; Friedrich and Laurent 2004), it is possible that the locust AL, by restructuring the odor representation through lateral network interactions, increases the distance between the representations of similar odors (i.e. odors that activate similar sets of ORNs) while causing dissimilar odors to converge in representation. Since the odor information available to PNs cannot exceed the information content of stimulus-evoked ORN activity, a theoretical ideal classifier could not improve its odor discrimination ability by using PN spikes rather than ORN spikes. However, any real classifier, such as the neural mechanism by which the locust brain deciphers PN activity, is imperfect, and hence stimulus separation by the AL may enhance the ability of such a classifier to discriminate among similar odors.

To investigate the functionality of the locust AL, we constructed a computational model of 90 PNs and 30 LNs described by Hodgkin-Huxley type kinetics. We show that in response to stimulation our model network captures the known physiological properties of the locust AL—20 Hz LFP oscillations, slow patterning, and the dynamic and fixed point behavior of large-scale network activity. Additionally, we test the ability of our network to discriminate among simulated odor stimuli to determine whether the dynamic code of the network leads to better stimulus discrimination than a simple combinatorial code. We also test the ability of our network to discriminate among stimuli that are encoded along the dimension of stimulus current intensity and determine the efficacy of the dynamic code versus the combinatorial code in this situation. Finally, we use principal component analysis to characterize stimulus separation and the dimensionality of the odor response in our model network.

2 Results

Our model network captures several of the known functional properties of the locust antennal lobe; we show the emergence of 20 Hz oscillations in the LFP, the existence of slow temporal patterning, and the qualitative agreement of principal component odor trajectories with those observed experimentally. Additionally, we examine the change in functionality of our model network after removal of various components. Finally, we test the ability of our model network to discriminate odors, both in the case where odors are represented in a combinatorial fashion (different odors are represented by stimulating different sets of PNs and LNs) and in the case where odors are represented as intensity distributions (different odors are represented by stimulating the same set of PNs and LNs but with different distributions of stimulus intensity). An odor is simulated by stimulating a set of 36 PNs and 12 LNs, which constitute approximately one-third of the total number of cells (see Methods of Bazhenov et al. 2001b).

There have been several previous studies of large-scale network models of the AL (Bazhenov et al. 2001b; Bazhenov et al. 2001a; Sivan and Kopell 2006). It is important to note that, in contrast to the locust AL model of Bazhenov et al. (2001a, b), our model has sparse connectivity among PNs, weak PN-PN synapses, and a prolonged rise and decay time of ORN input to PNs to match the time course observed experimentally (Wehr and Laurent 1999). We found that sparse connectivity and weak coupling between PNs were required to obtain the uncorrelated 2–4 Hz spontaneous activity seen in locust PNs (Perez-Orive et al. 2002), while the interplay between the time course of ORN input and the slow inhibitory current was essential in generating slow temporal patterning in our model.

2.1 Choice of ORN input time-course

We chose our ORN input time-course so that stimulus-onset and offset induced transient activity in our model qualitatively

matched the prolonged responses seen *in vivo* (Mazor and Laurent 2005—Fig. 1; Laurent et al. 1996—Fig. 5). More specifically, we chose ORN time scales on the order of 400 ms (see Methods) to ensure that, consistent with experiment, PN activity in our network built up gradually over ~500 ms upon odor onset, and lasted more than ~500 ms after odor offset.

It is important to note that this dynamical feature is not fully represented in the earlier models of Bazhenov et al. (2001a, b). In contrast, the models of Bazhenov et al. (2001a, b) display PN activity which saturates very quickly (<500 ms) after odor onset, and decays very quickly after odor offset. We believe it is likely that the faster ORN input-time-course (~100 ms) used in the Bazhenov et al. model is primarily responsible for the fast PN onset and offset transients produced by this model. This observation was supported by our experience developing our AL model.

Although the envelope of ORN input played a crucial role in producing the slow temporal structure of PN responses in our network, we note that mechanistically our slow patterning differs in a fundamental way from that seen in Sivan and Kopell's (2006) model. Sivan and Kopell's model (2006) recreated slow patterning by temporally modulating ORN input to PNs in an odor-specific and PN-specific manner, while our ORN input was modeled using a single slow rise time and a single slow decay time, both of which were uniform across PNs and odors. We chose this single slow rise time and decay time in order to emphasize and distill the theoretical possibility that the variety of slow patterns observed in the AL are a result of dynamical interplay among neurons within the network, rather than a consequence of a feed-forward process with structured inputs.

2.2 Choice of sparse network connectivity

We explored a wide range of connectivity schemes before arriving at our final set of cell-cell connection probabilities

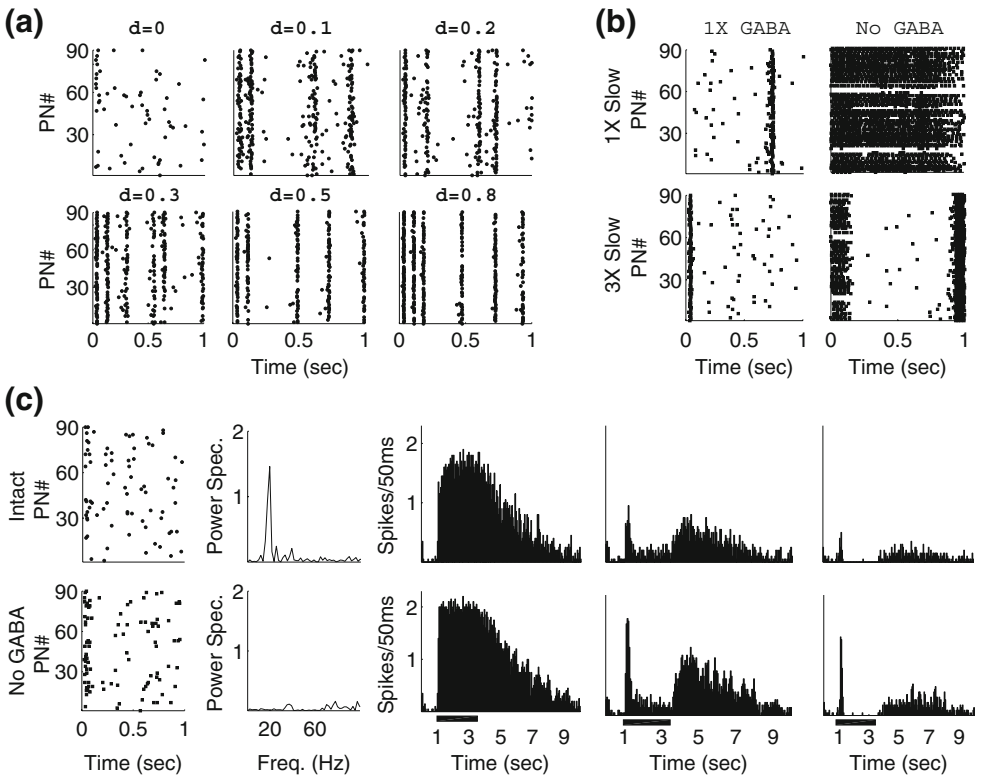

Fig. 1 Network connectivity. In order to place the network in the appropriate dynamic regime, PN-PN connectivity must be sparse, while connection probabilities involving LNs can vary broadly. (**a**) Sample spike rasters of background PN activity from networks with progressively denser connectivity. The cell type specific connection probabilities associated with each raster are given by PN-PN = 0.1 + d, PN-LN = 0.1 + d, LN-PN = 0.15 + d, and LN-LN = 0.25 + d. (**b**) Sample spike rasters of background PN activity from a network in which only PN-PN connectivity is dense (0.5) while connections involving LNs remain sparse (PN-LN = 0.1, LN-PN = 0.15, LN-LN = 0.25). The strength of PN-PN synapses has been weakened as much as possible while maintaining appropriate dynamical behavior under stimulation. The rasters shown are from networks with or without GABAergic transmission, and in the presence of normal- or triple-strength slow inhibitory synapses. (**c**) Plots from a network in which connection probabilities involving LNs are dense (0.5) while the PN-PN connection probability remains sparse (0.1). The strength of LN inhibition and PN excitation to LNs has been weakened to compensate for the increased synaptic density (top row—intact network, bottom row—no GABAergic transmission). From left to right: spike rasters of spontaneous PN activity, power spectrum of the network LFP under stimulation, trial-averaged spike rasters from three sample PNs (20 trials, black bar represents stimulus)

(PN-PN=0.1, PN-LN=0.1, LN-PN=0.15, LN-LN=0.25). Our goal was to choose a set of sparseness coefficients which would allow our network to behave in a physiologically reasonable manner when undriven (i.e. in background), while still producing the appropriate phenomena when driven. Figure 1 shows spike rasters of PN activity during background for networks with progressively denser connectivity (the density parameter **d** represents the number added to the connection probabilities mentioned above to yield the new connection probabilities, so **d=0** corresponds to the probabilities above and **d=0.8** corresponds to nearly all-to-all connectivity). While **d=0** yields the scarce, uncorrelated PN firing seen *in vivo* (Perez-Orive et al. 2002), as **d** is increased spontaneous PN activity becomes more frequent and more synchronized, suggesting that some sparsity in network connectivity may be required in order to place the network in the appropriate dynamic regime. Reasonable background activity can also be obtained by allowing dense connectivity while increasing spontaneous LN activity, but this leads to the emergence of subthreshold membrane potential oscillations in PNs and a 20 Hz peak in the LFP, which are not observed experimentally (Laurent and Davidowitz 1994; Mazor and Laurent 2005).

Rather than raising all connection probabilities simultaneously, we also examined network behavior in the presence of abundant PN-PN synapses while synapses involving LNs remained scarce. Selectively increasing the PN-PN connection probability without reducing the strength of PN-PN synapses leads to unrealistic spontaneous activity very similar to that seen in Fig. 1a; thus, as we progressively increased the density of PN-PN connections, we concurrently weakened the strength of PN-PN synapses as much as possible while still preserving appropriate dynamical network behavior under stimulation (so that sufficient lateral excitation existed within the network to allow the coherent bursts of PN spikes that are needed to globally synchronize LN activity and generate 20 Hz oscillations in the LFP; see Discussion). Figure 1(b) shows rasters of spontaneous PN activity in the case that the PN-PN connection probability was set to 0.5 (similar results were seen for other dense PN-PN connection probabilities); while background activity is relatively reasonable (other than rare synchronized bursts of PN spikes) in the intact network, the removal of fast GABA synapses leads to long bouts of high-frequency PN spiking in background, which is inconsistent with experimental recordings from locust PNs after infusion of the GABA antagonist picrotoxin into the AL (MacLeod and Laurent 1996; MacLeod et al. 1998). To assess whether such network behavior could be rectified by amplifying slow inhibition, we tripled the strength of slow inhibitory synapses within the network; while enhanced slow inhibition shortened the observed epochs of high-frequency spontaneous PN activity, it could not eliminate them. It therefore appears that scarcity in the connections among PNs is required to produce physiologically reasonable dynamical behavior.

Sparse connectivity over all cell type pairs, however, is not required to obtain the correct dynamic regime—specifically, only sparse PN-PN connections are needed. We experimented with a network in which the PN-PN connection probability was 0.1 but all others were set to 0.5, and we found that, after appropriately decreasing the strength of LN inhibition and PN excitation to LNs, the network remained in the same dynamic regime, and was still capable of producing the results presented here. Figure 1(c) shows that prominent features of network dynamics (low and uncorrelated spontaneous PN activity, GABA-dependent 20 Hz LFP oscillations, slow patterned PN responses that are unaffected by the removal of fast GABA-mediated inhibition) are preserved in the presence of dense connectivity involving LNs. Due to a lack of any published data on locust AL connectivity, we arbitrarily chose the LN-PN, PN-LN, and LN-LN connection probabilities mentioned above. However, we emphasize that all results reported below can be reproduced when connectivity among PNs is sparse (~0.1) while other connection probabilities remain dense (~0.5). It is important to note that PN spike rasters from the model of Bazhenov et al. (2001b—Fig. 3B, 2001a—Fig. 5) seem to show that PNs in their model either rarely fire in background or have relatively high spontaneous spike rates (~10–20 Hz), which is likely a consequence of their dense and strong PN-PN synapses and is inconsistent with experiment (Perez-Orive et al. 2002). In our experiments with our model, we also observed that dense and strong PN-PN coupling leads to similar behavior—the network is either too strongly inhibited in background or spontaneous PN firing rates are physiologically unreasonable.

2.3 LFP oscillations

Upon odor stimulation, strong 20 Hz oscillations can be seen in the LFP of the AL, as measured from the mushroom body (Laurent and Davidowitz 1994). Presumably, the LFP represents the average membrane potential of the axons of a large number of the PNs converging onto the mushroom body (Laurent and Naraghi 1994). We approximated the LFP signal corresponding to our model network by averaging the membrane potential of all 90 PNs in the network. Figure 2 shows the LFP trace of our network, as well as the integrated power in the 15–25 Hz range and the power spectrum during stimulation. Shortly after stimulus onset, the LFP of the intact network exhibits strong 20 Hz oscillations which decay approximately 1 s after onset and disappear after stimulus offset, in accordance with experiment (Mazor and Laurent 2005). In agreement with MacLeod and Laurent (1996), removal of GABA input to the PNs to simulate picrotoxin application leads to a loss of

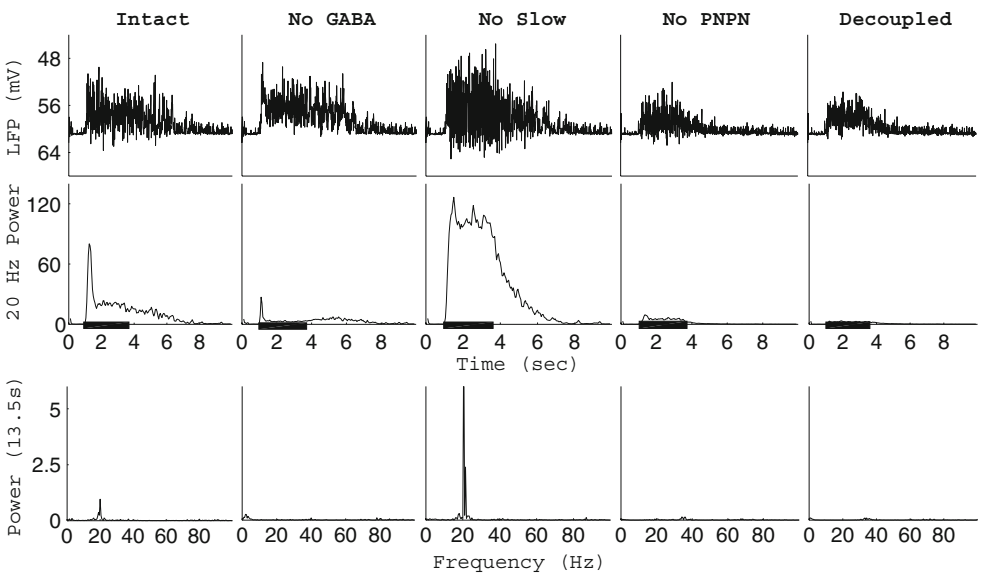

Fig. 2 Emergence of 20 Hz LFP oscillations. Oscillations in the LFP of the intact network, network with GABA removed, network with no slow inhibition, network with no PN-PN connections, and the completely decoupled network during stimulus presentation (stimulus duration indicated by the black bar). An LFP trace of the network is presented (top row), along with integrated power in the 15–25 Hz range (middle row, 200 ms sliding window, 50 ms step size, 20 trial average), and the power spectrum of the LFP during stimulus presentation (bottom row, single trial)

20 Hz synchrony. The removal of slow inhibition from the network leaves the LFP oscillations intact (in fact, PN synchrony is increased), while blocking PN-PN synapses or completely decoupling the network abolishes oscillatory synchrony.

2.4 Slow temporal patterning

The AL exhibits reproducible odor- and PN- specific temporal spiking patterns in response to odor presentation (Laurent et al. 1996). This slow patterning phenomenon is evident in our model network. Figure 3 shows trial-averaged spike histograms from four sample PNs in our model network in response to a single simulated odor stimulus (the histograms represent the number of spikes in 50 ms time bins averaged over 20 stimulus trials). PN1 responds vigorously throughout the period of stimulation, with the response gradually decaying after stimulus offset. PN2, on the other hand, exhibits a strong response at stimulus onset, responds moderately throughout the duration of the stimulus, and subsequently exhibits a strong response after stimulus offset. PN3 has similar strong onset and offset responses, but after the onset response PN3 does not respond at all throughout the duration of the stimulus. In contrast, PN4 does not exhibit any response above background to the stimulus.

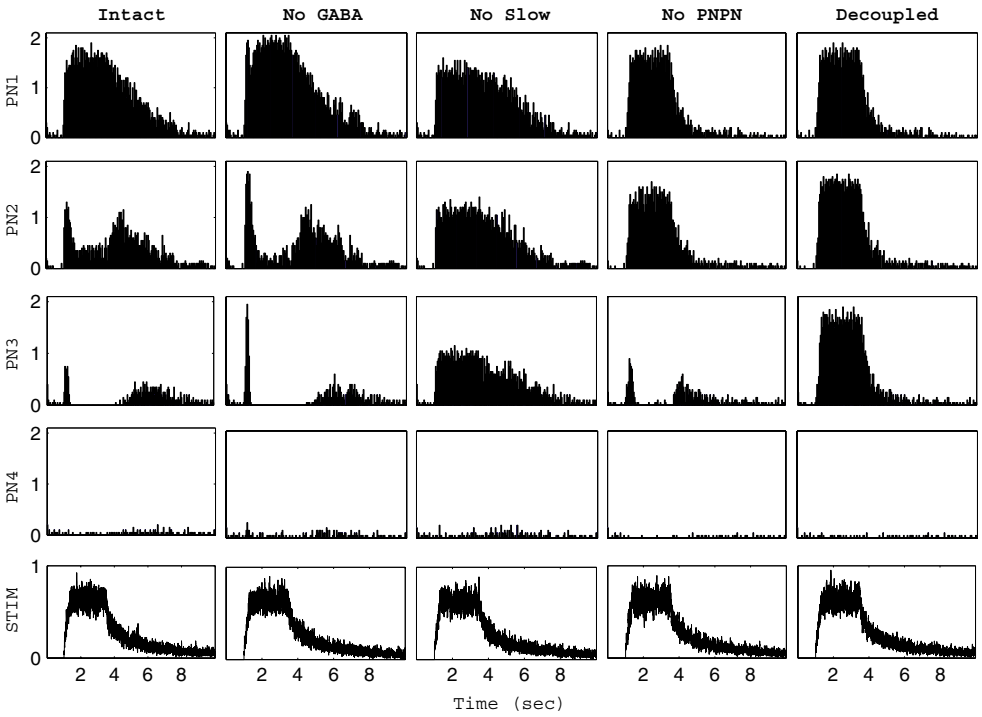

Fig. 3 Slow temporal patterning. Slow temporal response patterns of four PNs (rows) in the case of the intact network, network with no GABA, network with no slow inhibition, network with no PN-PN connections, and completely decoupled network (columns) in response to a single simulated odor (stimulus time course shown in the bottom row). The histograms represent the number of spikes (averaged over 20 trials) in 50 ms time bins

Experimentally, application of the GABA antagonist picrotoxin to the AL results in the disappearance of oscillations in the LFP, but slow temporal patterning remains intact (MacLeod and Laurent 1996; MacLeod et al. 1998). In accordance with experiment, when GABA input to the PNs is removed from our network, the slow temporal character of PN response patterns is unchanged. Removal of slow inhibition, however, results in loss of the fine temporal structure of PN responses; without slow inhibition, PNs either respond throughout the period of stimulation or do not respond at all. Blocking PN-PN synapses alters the slow temporal structure of PN responses but does not abolish the modulation of PN responses over slow time scales. Additionally, after stimulus offset PN spiking activity decays more steeply and quickly back to baseline firing rates. Completely decoupling the network leads to a loss of slow patterning as well as a short, steep decay of PN firing rates after stimulus offset.

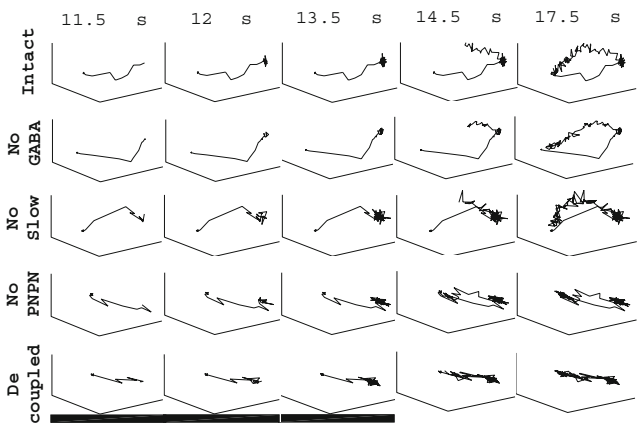

Fig. 4 Principal component trajectories. Principal component trajectories computed from PN firing rates (averaged over 20 trials) in response to a single simulated odor (stimulus duration indicated by the black bar). Trajectories were computed for the intact network (top row), the network with GABA input to the PNs removed (second row), the network with no slow inhibition (third row), the network with no PN-PN connections (fourth row), and the completely decoupled network with no cell-cell connections (bottom row)

2.5 Principal component analysis

One way in which to visualize salient features of total AL network activity is through principal component analysis. Using recordings from 99 PNs in response to presentation of a single odor, Mazor and Laurent (2005) performed principal component analysis on the matrix of trial-averaged PN firing rates as a function of time. Projection of the data onto the first three principal components yielded an odor response trajectory with several key properties : 1) a transient dynamic portion of the trajectory after stimulus onset; 2) approach of the trajectory to a fixed point reached approximately 1 s after stimulus onset; 3) stability of the trajectory at the fixed point until stimulus offset; 4) a transient dynamic deviation of the trajectory away from rest after stimulus offset; 5) gradual decay of the trajectory back to the network's resting state.

We performed principal component analysis on our network's matrix of trial-averaged firing PN firing rates as a function of time in response to a simulated odor stimulus. Additionally, we computed the principal component trajectories of our network's response to the same simulated odor after modifying network functionality via removal of various components. Principal component trajectories were computed for our model network in five scenarios : 1) fully intact network; 2) network with removal of GABA input to the PNs; 3) network with no slow inhibition; 4) network with no PN-PN connections; 5) completely decoupled network. The resulting trajectories are shown in Fig. 4.

The trajectory of our fully intact network captures the observed features of an experimentally computed odor-response trajectory; a fixed point is reached approximately 1 s after odor onset, and a transient deviation for approximately 1 s after stimulus offset occurs prior to a gradual decay to rest. Consistent with the preservation of slow patterning after removal of GABAergic transmission from the network, removal of GABA input to the PNs results in a stimulus-response trajectory exhibiting qualitatively similar behavior to that of the fully intact network. Removal of slow inhibition from the network, however, results in a drastic alteration of the response trajectory. The trajectory exhibits a short deviation and approach to a fixed point after stimulus onset; after stimulus offset, the loss of slow patterning causes the trajectory to essentially retrace its path back to rest. The removal of PN-PN connections from our model network results in a different type of alteration in the stimulus-response trajectory. The trajectory deviates from rest after stimulus onset and reaches a fixed point within 1 s, and after stimulus offset the trajectory experiences a short deviation prior to returning to rest. However, the trajectory returns to rest within 1 s after stimulus offset, in contrast to the trajectory of the fully intact network, which takes approximately 4 s to decay to the background state after stimulus offset. In comparison, the trajectory of the completely decoupled network reaches a fixed point approximately 1 s after stimulus onset and retraces its path back to the resting state within 1 s after odor offset.

2.6 Combinatorial odor discrimination

To test the ability of our network to discriminate among odors in various functional states, we employed a set of 31 simulated odors (each odor is represented as a different set of PNs and LNs that receive stimulus current). We ran 20 trials for each odor, and the 31 simulated odors were

presented to the model network in each of the five scenarios mentioned earlier. To assess the discrimination ability of the network for a given subset of the 31 odors, we computed odor templates for each odor being tested as the vector of trial-averaged PN firing rates as a function of time, and subsequently determined the fraction of test odor trials correctly classified by the network as a function of time (see Methods). The discrimination ability of the network for a set of simulated odors was determined as the average fraction of trials correctly classified by the network throughout the duration of the stimulus.

We computed the discrimination ability of our network in each of the five functional states mentioned earlier for a randomly selected subset of 5, 10, 15, 20, 25, and 31 odors from our entire simulated odor set of 31 odors. The results are presented in Fig. 5 (left panel). The fully intact network retains a high discrimination rate as the number of odors the network is required to differentiate is increased; additionally, removal of GABAergic transmission or removal of PN-PN connections from the network does not degrade the network's discrimination ability. Removal of slow inhibition from the network, however, causes the network's ability to discriminate odors to drop significantly as the number of odors the network is required to differentiate is increased. The completely decoupled network shows similar behavior to the network with no slow inhibition, although the drop in discrimination ability with number of simulated odors is more severe.

2.7 Intensity based odor discrimination

To test the ability of our network to discriminate stimuli along a coding dimension different from the combinatorial code assessed above, we selected a fixed set of 36 PNs and 12 LNs to receive stimulus current. We divided the cells into six groups, with each group receiving stimulus current at 100%, 90%, 80%, 70%, 60%, or 50% intensity (see Methods). A simulated odor was represented as a particular pattern of stimulus intensity distribution. We ran 20 trials for each of 18 simulated odors and assessed our network in each of five functional states.

Figure 5 (right panel) shows the discrimination ability of our network for a randomly selected subset of 6,12, and 18 simulated odors. In general, the network was unable to discriminate odors as precisely as in the case where odors were represented in a combinatorial manner, regardless of the functional state of the network. However, some striking differences were observed in discrimination ability among the various functional states of the network. While discrimination ability decreased as the number of odors the network was required to differentiate increased in each of the functional states, the network with no PN-PN connections and the completely decoupled network performed significantly better than the other functional states in the discrimination task. The fully intact network, the network with no GABA input to the PNs, and the network with no slow inhibition exhibited comparable performances in the discrimination task.

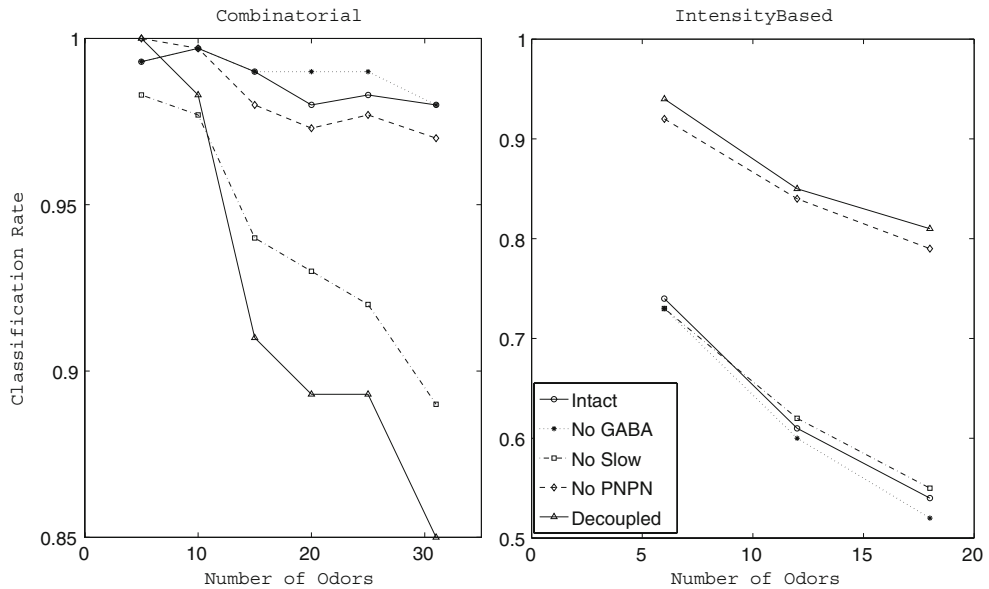

Fig. 5 Combinatorial vs. intensity-based odor discrimination. Time-averaged fraction of trials correctly classified by the network versus number of odors the network was required to discriminate (20 trials per odor) in the case of the intact network, network with no GABA, network with no slow inhibition, network with no PN-PN connections, and completely decoupled network. In the combinatorial case (left figure), a total of 31 simulated odors were used, with different stimuli represented by different sets of PNs and LNs receiving stimulus current. In the intensity case (right figure), a total of 18 simulated odors were used, with different stimuli represented by a fixed set of PNs and LNs receiving different distributions of stimulus current intensity. In both cases, subsets of odors were chosen randomly from the entire set. Similar results were seen regardless of the subsets chosen

Figure 6 shows the classification rate as a function of time of our model network in each of the five functional states, both in the case where the network was required to discriminate our entire set of 31 combinatorial stimuli and in the case where the network was required to discriminate our set of 18 intensity-based stimuli. As mentioned above, the intact network is better able to discriminate odors encoded in a combinatorial manner, while the decoupled network is more accurate in classifying odors encoded as intensity distributions. We also note that in the network with no PN-PN connections, the decay back to baseline in odor discrimination after stimulus offset is steeper than in the network with intact PN-PN synapses. Additionally, Fig. 6 shows that classification rate tends to roughly follow the stimulus time course; varying the time constants of stimulus rise and decay leads to corresponding alterations in the rise and decay of odor discrimination without affecting the classification rate at which odor discrimination plateaus (data not shown).

3 Discussion

Our model network exhibits 20 Hz LFP oscillations, slow temporal patterning, and transient and fixed point behavior of the principal component trajectory which are qualitatively similar to those observed within the locust AL (Mazor and Laurent 2005). We have provided evidence that, within our model, GABAergic inhibition provided by LNs is essential for 20 Hz PN synchrony, while the slow inhibitory current from LNs to PNs is crucial in generating the temporal pattern of PN responses. We also examined our model network after removing PN-PN connections and after complete decoupling, which indicated that PN-PN synapses were required to obtain the gradual decay profile of PN responses with stimulus decay. Furthermore, we showed that the completely decoupled network, providing an analog to the ORN representation of a stimulus, performed worse in stimulus discrimination than the intact network when odors were represented in a combinatorial manner. Since it is thought that odors are indeed represented in a combinatorial manner at the ORN level (Joerges et al. 1997; Vickers and Christensen 1998; Vickers et al. 1998; Malnic et al. 1999; Ache and Young 2005; Wang et al. 2003; Ng et al. 2002), this result suggests that AL network activity may aid in stimulus separation. Interestingly, however, the decoupled network was a more accurate classifier when stimuli were coded along the dimension of current intensity. We now examine these phenomena in more detail.

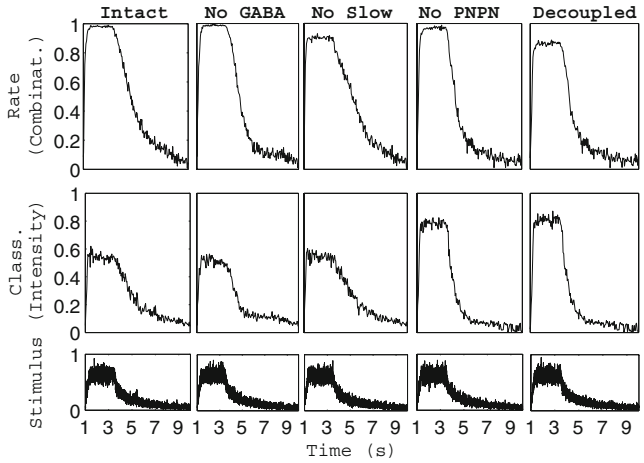

Fig. 6 Odor discrimination as a function of time. Fraction of trials correctly classified by the network as a function of time for the network in each of five functional states (columns). The discrimination task was performed among our set of 31 odors encoded in a combinatorial manner (top row) or our set of 18 odors encoded as intensity distributions (bottom row). The fraction of trials correctly classified by the network was computed in 50 ms time bins (see Methods)

3.1 Oscillations and slow patterning

Upon presentation of a simulated odor, the PNs in our network receiving stimulus current begin firing sodium spikes. This PN firing induces EPSPs in the postsynaptic LNs through fast cholinergic synapses, and in turn the LNs fire slow calcium spikes. These slow calcium spikes activate GABA synapses and result in the activation of fast IPSPs in postsynaptic PNs, delaying subsequent PN spikes and giving rise to the 50 ms oscillation time scale. In addition to PN influence, LN dynamics were also governed by fast GABA interactions with other LNs. Sets of active LNs suppress the remaining LNs, but the calcium dependent potassium current becomes active in an LN after it spikes several times, leading to spike adaptation. This spike adaptation releases inhibited LNs, and the released LNs begin spiking and previously spiking LNs are suppressed. Thus, the set of active LNs evolves dynamically—from the set of LNs synapsing onto a given PN, the number which are active varies with time (Bazhenov et al. 2001b).

Fast GABA synapses, however, are insufficient to create the slow temporal patterns seen in PN responses, both in our network and in the locust AL (MacLeod and Laurent 1996; MacLeod et al. 1998). To generate slow patterning, we included a slowly activating inhibitory current from LNs to PNs using a model of $GABA_B$ receptor kinetics (Destexhe et al. 1996; Dutar and Nicoll 1988) modified to cause significant receptor activation after approximately three presynaptic LN calcium spikes (Bazhenov et al. 2001a). In accordance with the experimentally observed time course of ORN responses to odor stimuli (Wehr and Laurent 1999), the temporal profile of our ORN input was less steep than that of Bazhenov et al. (2001a, b). If t_o is the

time of stimulus onset and t_d the time of stimulus offset, then the odor-evoked input rate of ORN spikes to a stimulated cell in our network was given by $R(t) = r_m exp\left(-(t-(t_o+s))^2 \Big/ c_1\right)$ for $t = t_o$ to $t = t_o + s$, by $R(t) = r_m$ for $t = t_o + s$ to $t = t_d$, and $R(t) = r_m exp(-sqrt(t-t_d)/c_2)$ for $t > t_d$, where $s = 400\ ms$ was the rise time, $c_1 = 100{,}000$, $c_2 = sqrt(1000)$ were the scaling constants, and r_m was the maximal stimulus-evoked ORN input rate. Following the stimulus time course, the slow patterning of the response of an active PN generally consisted of three distinguishable phases: 1) response to stimulus onset, during which the firing rate of the PN changed gradually (corresponding to the initial dynamic portion of the network PCA trajectory); 2) approach to a steady-state firing rate within 1 s (corresponding to the fixed point in the network PCA trajectory); 3) response to stimulus offset, during which the firing rate changed gradually and then returned to baseline (corresponding to the offset dynamic portion of the network PCA trajectory). During each phase, the firing rate of each responding PN was determined by the competition between slow inhibitory input and net excitatory input. As the mean stimulus current level changed, the set point resulting from this antagonism shifted and the firing rate of each PN changed accordingly. When the mean stimulus current level was constant, a few hundred milliseconds were required before the net effect of slow inhibition and excitation to each PN reached a steady-state (due to the time course of the slow inhibition) and each PN assumed a fixed firing rate. Thus, our model postulates that the temporal patterning of locust PN odor responses is a consequence of the interaction between the time course of the ORN odor response and a slow inhibitory mechanism within the AL network.

Although a slow inhibitory current such as the one incorporated into our model has not been found in the locust AL, the preservation of slow patterning after application of a $GABA_A$ receptor antagonist (MacLeod and Laurent 1996; MacLeod et al. 1998) indicates the presence of some uncharacterized mechanism capable of modulating PN firing rates on slow time scales. In the moth, PNs are equipped with a calcium-dependent potassium current capable of causing slow changes in PN firing rates (Mercer and Hildebrand 2002a, b). Sivan and Kopell (2006) reproduce slow patterning in a model of the locust AL by introducing variability in the envelope of ORN input to PNs and equipping PNs with a calcium-dependent potassium current. However, intracellular recordings from locust PNs show prolonged epochs of hyperpolarization in PNs that showed no previous spiking activity (Laurent et al. 1996), indicating the presence of a synaptic slow inhibitory mechanism rather than an intrinsic one. Similar to the locust, the honeybee AL also exhibits picrotoxin-sensitive global LFP oscillations (Stopfer et al. 1997) in conjunction with a second, picrotoxin-resistant inhibitory mechanism (Sachse and Galizia 2002). Furthermore, experiments show the persistence of a slow, GABA-mediated inhibitory current in cultured honeybee antennal lobe neurons after application of picrotoxin (Barbara et al. 2005; see Fig. 4), implying the existence of a synaptic inhibitory mechanism acting through picrotoxin-resistant GABA receptors with a time course similar to that of the slow receptors used in our model.

3.2 Functional states of the network

When GABA input to the PNs is removed, the network behaves in a manner similar to that of the intact network (as seen in the spike histograms and PCA trajectories), except for the disappearance of the 20 Hz oscillations in the LFP. This implies that fast GABA currents serve to synchronize PN activity but do not affect PN firing rates, as shown *in vivo* (MacLeod and Laurent 1996; MacLeod et al. 1998). This occurs because a PN fires at most once or twice in any 50 ms epoch, and thus the short (50 ms) time scale of a GABA-induced IPSP only delays a PN spike rather than preventing it. Removal of slow inhibition, however, eliminates the slow temporal structure of PN responses; without the presence of a slow inhibitory current to balance the excitatory input to a PN, the PN either does not respond at all or its firing rate faithfully reflects the time course of the stimulus current. In the network PCA trajectory, the loss of slow patterning is evident in the lack of a robust deviation after stimulus offset.

Removal of PN-PN connections from the network leads to a steeper decay back to baseline of PN firing rates after stimulus offset. Since the only excitatory input that responding PNs receive is stimulus current, once this current drops below a certain threshold the lack of reverberating excitation normally mediated by PN-PN connectivity causes PNs to simply cease firing. This phenomenon is evident in the PN spike histograms as well as in the relatively rapid return to rest of the network PCA trajectory after stimulus offset. Additionally, shutting off PN-PN synapses results in a loss of LFP oscillations; although individual PNs still tend to exhibit oscillatory spiking (data not shown), LN input alone is insufficient to synchronize activity across PNs. Coherent network oscillations are the result of alternating PN and LN activation—synchronized firing of a large number of PNs leads to synchronized activation of a large number of LNs , which in turn inhibits PN firing for ~50 ms until the next burst of PN spikes. It appears that lateral excitatory connections are required to elicit the synchronized burst of PN spikes needed to organize coherent LN activation; thus, our model predicts that PN-PN coupling must exist within the locust AL to allow global network oscillations, but that PN-PN

synapses must be sparse and weak to place the network in the appropriate dynamic regime (see Results). Since slow inhibitory synapses remain functional, however, the network is still capable of modulating PN firing rates on slow time scales, as apparent from the spike histograms and the fact that the network PCA trajectory deviates after stimulus offset rather than retracing its path back to the resting state. The completely decoupled network, as expected, shows no LFP oscillations or slow patterning; the firing rates of stimulated PNs follow the stimulus time course and decay steeply back to baseline after stimulus offset, while PNs that do not receive stimulus current do not respond.

3.3 Odor discrimination

We assessed the stimulus discrimination ability of our model network using two different paradigms of odor stimuli : 1) combinatorial-based, where different odors were represented as distinct subsets of stimulated cells; 2) intensity-based, where different odors were represented by stimulating the same subset of cells with different distributions of stimulus current intensity. Regardless of functional state, our model network was in general better able to discriminate among stimuli in the combinatorial paradigm than in the intensity paradigm. Since it is likely that early olfactory systems are optimized to encode stimuli represented in a combinatorial manner (Joerges et al. 1997; Vickers and Christensen 1998; Vickers et al. 1998; Malnic et al. 1999; Ache and Young 2005; Wang et al. 2003; Ng et al. 2002), it is plausible that the locust AL network exhibits similar behavior.

When odors were represented in a combinatorial manner, the intact network discriminated odors more accurately than the completely decoupled network, suggesting that the transformation of the ORN sensory code occurring in the locust AL does indeed enhance stimulus separation. The network with PN GABA receptors blocked performed comparably to the intact network, raising a question as to the purpose of synchronized oscillations in odor discrimination. MacLeod et al. (1998) recorded from PNs *in vivo* and found that picrotoxin application to abolish oscillations did not degrade the ability of single PN spike trains to distinguish odors. However, they also recorded from higher order neurons in the locust olfactory pathway and found that these neurons showed less stimulus selectivity and were unable to discriminate chemically similar odors after picrotoxin infusion into the AL. Furthermore, electrophysiological recordings from locust Kenyon cells, the neurons of the mushroom body that read PN activity, show that these cells possess active dendritic conductances and short integration windows and can thus act as coincidence detectors of synchronized PN input (Perez-Orive et al. 2004). In a behavioral assay using honeybees, Stopfer et al. (1997) showed that injection of picrotoxin into the AL impaired the ability of the animals to discriminate among chemically similar odors, and computational modeling by Sivan and Kopell (2004) describes a mechanism by which synchronized oscillations in the locust AL could enhance discrimination of similar stimuli by downstream neurons. Together, these results suggest that while GABA-induced oscillatory synchrony may not affect PN information content or aid in stimulus separation, it likely plays a crucial role in the mechanism by which downstream neurons decode PN activity.

In contrast, removal of slow inhibition from our network results in an impairment in the ability of the network to discriminate among stimuli represented in a combinatorial manner, supporting the notion that slow temporal patterning is required for decorrelation and optimal stimulus separation. Blocking PN-PN synapses in the network did not degrade odor discrimination during stimulus presentation. However, after stimulus offset the discrimination ability of the network decayed faster than in the intact network, implying that PN-PN connectivity in the locust AL may serve to prolong the neural representation of an odor stimulus immediately after removal of the odor from the animal's sensory environment.

Interestingly, when odors are represented as intensity distributions, the completely decoupled network discriminates among stimuli more accurately than the functionally intact network. The network lacking PN-PN synapses behaves similarly to the decoupled network, while blocking PN GABA receptors or shutting off slow inhibition resulted in networks that distinguished odors much like the intact network, indicating that PN-PN coupling diminishes the ability of the network to discriminate intensity-coded odors. Since varying the concentration of a given odor is thought to modulate the firing rates of responding ORNs *in vivo* (de Bruyne et al. 2001; Wang et al. 2003; Friedrich and Korsching 1997; Meister and Bonhoeffer 2001), we can interpret our intensity-coded stimuli as representing different concentrations of the same odor, and our results then imply that PN-PN coupling augments the concentration invariance of the locust AL's odor representation. In fact, ORNs (represented by the completely decoupled network) would seem more sensitive to changes in stimulus intensity than the AL. Our odor discrimination results therefore suggest that AL network activity in the locust enhances the animal's ability to discriminate among different odors while minimizing its sensitivity to precise odor concentration. However, a potential caveat to this reasoning is that increasing odorant concentration in experiments tends to not only modulate ORN firing rates but also leads to the recruitment of additional glomerular input channels (Friedrich and Korsching 1997; Rubin and Katz 1999; Johnson and Leon 2000; Fuss and Korsching 2001; Meister

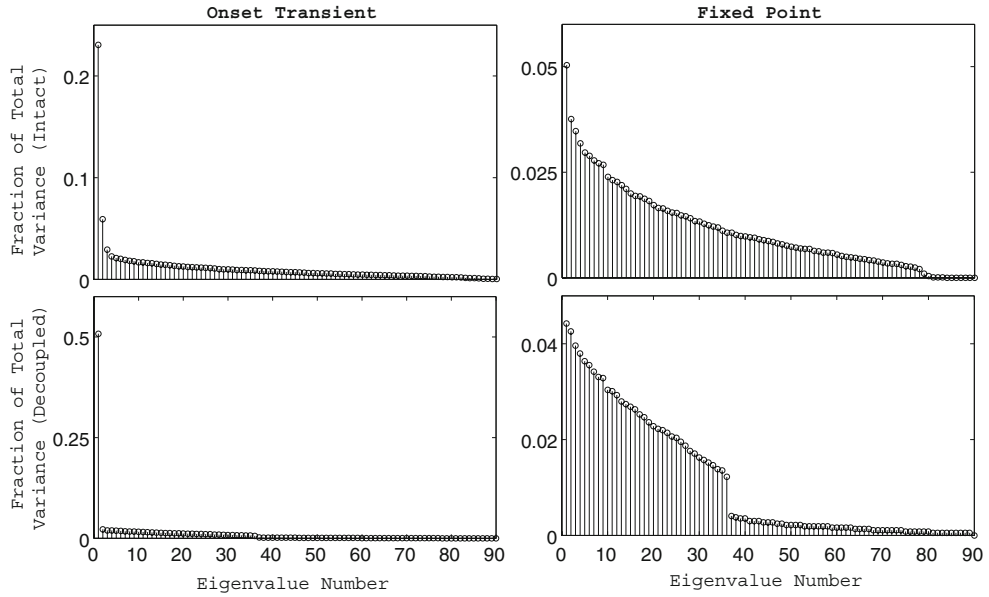

Fig. 7 Dimensionality of the odor representation. Fraction of the total variance in the PN firing rate data captured by each principal component vector during an odor response. The fraction of data variance captured by a principal component was computed as the magnitude of the corresponding eigenvalue normalized by the sum of the magnitudes of all ninety principal component eigenvalues. We performed principal component analysis and computed the distribution of total data variance over the resulting principal components during the transient portion of the odor response (1–2 s, left column) and during the fixed point (2.5–3.5 s, right column) for both the intact network (top row) and the completely decoupled network (bottom row)

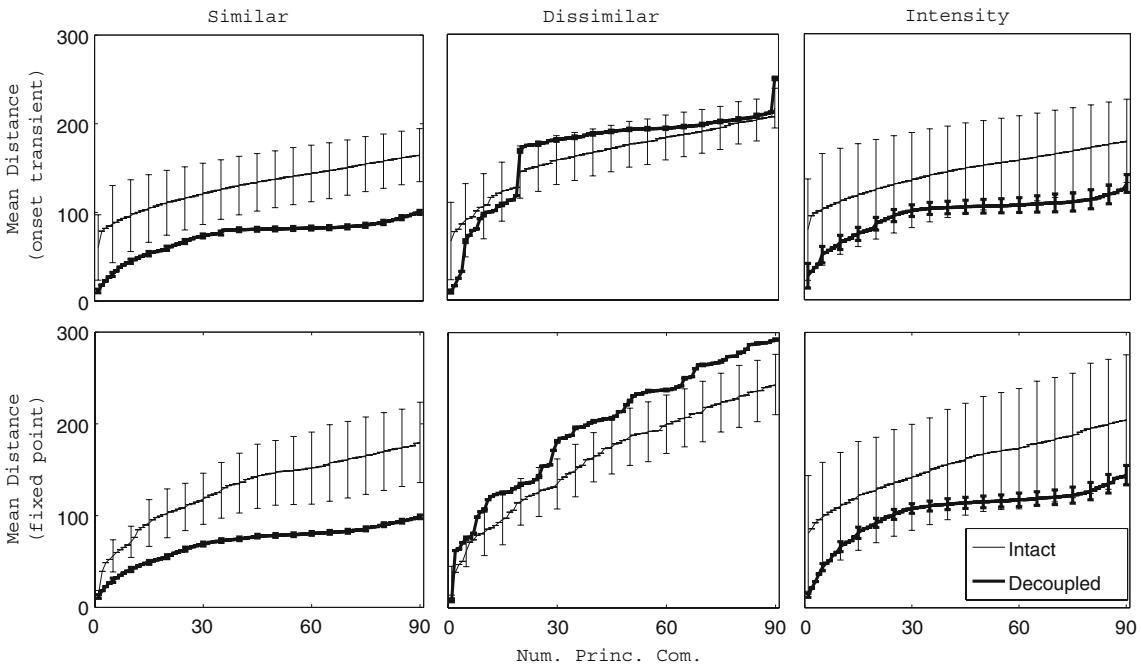

Fig. 8 Distance between the principal component trajectories of two odors. Time-averaged Euclidean distance between the principal component trajectories of two odors plotted as a function of the number of principal components used in the computation (50 ms time bins). For a given (i,j) odor pair, the time-averaged intertrajectory distance during the onset transient (top row, 1–2 s) or fixed point (bottom row, 2.5–3.5 s) was computed between each trial of odor i and each trial of odor j (20 trials per odor). The plots show the time-averaged distance between a trial of odor i and a trial of odor j averaged over all possible trial-trial pairs, and the error bars represent the standard deviation of the trial-trial distance. The analysis was performed for two similar combinatorially coded odors (left column), two dissimilar combinatorially coded odors (middle column), and two intensity coded odors (right column) in the case of the intact network as well as the completely decoupled network. Trajectories of trials from each odor pair were projected onto the same principal components to enable computation of intertrajectory distances

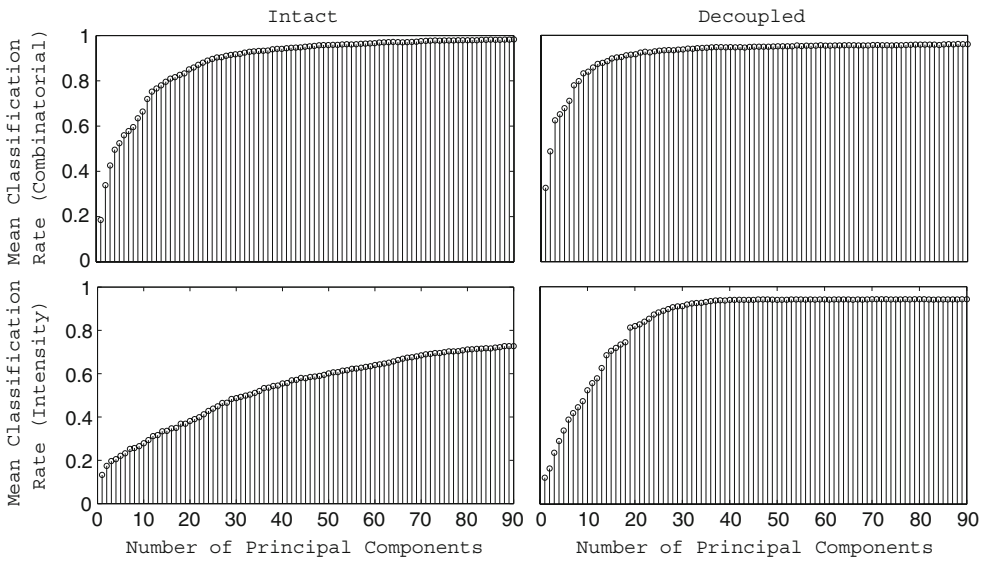

Fig. 9 Odor discrimination using a varying number of principal components. Time-averaged fraction of trials correctly classified by the network during the fixed point period of the odor response as a function of the number of principal components used in the classification task. The discrimination task was performed for 15 odors coded in a combinatorial manner (top row) and 10 odors coded as intensity distributions (bottom row) using both the intact network (left column) and the completely decoupled network (right column). In each discrimination task, odor trajectories were all projected onto the same principal components and the classification rate was determined as described in the Methods (except using the principal component trajectories rather than the original firing rate trajectories) using a varying number of principal components

and Bonhoeffer 2001; Wachowiak and Cohen 2001; Sachse et al. 1999; Galizia et al. 2000), indicating that the ORN representation of stimulus concentration may include a combinatorial component, and thus may not be as simple as the scheme suggested by our intensity-coded paradigm.

Mazor and Laurent (2005) computed odor discrimination as a function of time from experimentally obtained locust PN firing rate vectors, and they found a slightly reduced discriminability during the fixed point epoch of the odor response, a feature not observed in our model (Fig. 6). Mazor and Laurent (2005), however, used data from ~10% of the total number of PNs in the locust AL to compute their firing rate vectors, while we use data from all PNs in our network; it may be the case that during the fixed point epoch more PNs are required to adequately discriminate among odors, and therefore the issue of size of data set in relation to the slight reduction in classification rate deserves further examination. It is also possible that this reduction in classification rate is a result of receptor adaptation; if we included receptor adaptation effects in the time course of our ORN input (so that stimulus current amplitude began to decay to a new steady-state 0.5–1 s after onset) it may be the case that odor discrimination (as a function of time) would exhibit a slight decrease during the fixed point epoch in a manner similar to that observed by Mazor and Laurent (2005). While prolonged recordings from locust ORNs to show receptor adaptation have not been performed, spike frequency adaptation has been shown to occur in fly ORNs (de Bruyne et al. 1999).

3.4 High dimensional odor representations

In order to study the differences in the ways in which the intact network and the completely decoupled network encode an odor stimulus, we used PCA to characterize the dimensionality of the odor representation in the two networks. For each of the two networks, we performed PCA on the matrix of PN firing rates versus time both during the initial transient dynamic portion of the odor response (1–2 s) and during the fixed point epoch of the odor response (2.5–3.5 s). We computed the fraction of the total data variance captured by each of the principle components as the magnitude of the eigenvalue corresponding to each principle component normalized by the sum of the magnitudes of the eigenvalues of all ninety principle components (Fig. 7). If we view the time-dependent network trajectory during the odor response as a manifold in 90-dimensional PN space (where each axis in the space represents the firing rate of one of the PNs in the network), we can interpret the dimension of this manifold as the dimensionality of the network's odor representation. Additionally, we can obtain an approximation of the dimensionality of the odor manifold by estimating the number of principle components that make a significant contribution to the total data variance. As shown in Fig. 7, during the initial transient dynamic period of the odor response the dimensionality of the odor manifold is relatively low for both the intact and decoupled networks, although even at this stage more principal components

seem to contribute to the odor response of the intact network than to that of the decoupled network. During the fixed point, however, we observe a more striking difference between the intact and decoupled networks. In the decoupled network, the contribution of each principal component to the total data variance drops abruptly after the 36th eigenvalue, in accordance with the fact that only 36 PNs receive stimulus current and each neuron in the network is synaptically isolated from every other neuron. In the intact network, the contribution of each principal component to the total data variance exhibits a gradual decay profile, indicating that more than 36 principal components are required to adequately capture the odor response data. These results suggest that the dimensionality of the odor representation is higher in the intact network than in the decoupled network, which may have consequences in terms of odor discrimination.

To assess stimulus separation and its relation to odor discrimination in our network, we computed the time-averaged Euclidean distance between the principal component trajectories of two odors for three different odor pairs. For each odor pair, we calculated the time-averaged distance between the principal component trajectories of each trial of one odor and each trial of the other odor. The intertrajectory distances were averaged over all possible trial-trial pairs, and the resulting means and standard deviations are shown in Fig. 8. The intact network appears to separate combinatorially similar odors better than the decoupled network, while the opposite holds in the case of combinatorially dissimilar odors, and comparable stimulus separation is seen between the intact and decoupled networks for the pair of intensity-coded odors. In the combinatorial case, the increased stimulus separation seen in the intact network for similar odors is consistent with the fact that the intact network discriminates among combinatorially-coded odors more accurately than the decoupled network. In the intensity case, the ability of the decoupled network to perform more accurate odor discrimination than the intact network could be related to the large variance in stimulus separation by the intact network as opposed to the comparatively small variance in the stimulus separation data of the decoupled network. Additionally, stimulus separation is more invariant across different odor pairs for the intact network than for the decoupled network, supporting the idea that, as seen in the fly (Bhandawat et al. 2007), AL network activity separates the neural representations of similar odors while causing dissimilar odors to converge in representation, producing more uniform distances between odors. We also note that the intact network tends to exhibit increased stimulus separation with every additional principal component utilized in the computation, while stimulus separation by the decoupled network tends to saturate prior to exhausting all potential principal component dimensions. It is therefore possible that stimulus separation, dimensionality of the odor representation, and odor discrimination are intimately connected.

To further probe the link between stimulus discrimination and the dimensionality of the odor manifold in our network, we computed the correct classification rate of the intact and decoupled networks in distinguishing among 15 combinatorial odors or 10 intensity-coded odors as a function of the number of principal components used in the discrimination task (the classification rates were determined as described in the Methods, except we used the projected principal component trajectories rather than the original PN firing rate trajectories). The results of the analysis during the fixed point epoch of the odor response are plotted in Fig. 9 (similar results were obtained during the onset transient). The classification rate of the decoupled network seems to plateau at approximately 36 principal component dimensions, while the intact network shows no such saturation; to the contrary, odor discrimination by the intact network improves with every additional principal component dimension used in the task. Thus, not only is the dimensionality of the odor manifold higher in the intact than in the decoupled network, it appears that these extra dimensions contribute to the intact network's ability to separate stimuli and perform odor discrimination.

References

Ache, B., & Young, J. (2005). Olfaction: diverse species, conserved principles. *Neuron, 48*, 417–430. doi:10.1016/j.neuron.2005.10.022.

Axel, R. (1995). The molecular logic of smell. *Scientific American, 273*, 154–159.

Barbara, G., Zube, C., Rybak, J., Gauthier, M., & Grünewald, B. (2005). Acetylcholine, GABA and glutamate induce ionic currents in cultured antennal lobe neurons of the honeybee, *Apis Mellifera*. *Journal of Comparative Physiology. A, Sensory, Neural, and Behavioral Physiology, 191*, 823–836. doi:10.1007/s00359-005-0007-3.

Bazhenov, M., Timofeev, I., Steriade, M., & Sejnowski, T. (1998). Cellular and network models for intrathalamic augmenting responses during 10 Hz Stimulation. *Journal of Neurophysiology, 79*, 2730–2748.

Bazhenov, M., Stopfer, M., Rabinovich, M., Abarbanel, H., Sejnowski, T., & Laurent, G. (2001a). Model of cellular and network mechanisms for odor-evoked temporal patterning in the locust antennal lobe. *Neuron, 30*, 569–581. doi:10.1016/S0896-6273(01)00286-0.

Bazhenov, M., Stopfer, M., Rabinovich, M., Huerta, R., Abarbanel, H., Sejnowski, T., et al. (2001b). Model of transient oscillatory synchronization in the locust antennal lobe. *Neuron, 30*, 553–567. doi:10.1016/S0896-6273(01)00284-7.

Bhandawat, V., Olsen, S., Gouwens, N., Schlief, M., & Wilson, R. (2007). Sensory processing in the Drosophila antennal lobe increases reliability and separability of ensemble odor representations. *Nature Neuroscience, 10*, 1474–1482. doi:10.1038/nn1976.

Costanzo, R., & Morrison, E. (1989). Three-dimensional scanning electron microscopic study of the normal hamster olfactory epithelium. *Journal of Neurocytology, 18*, 381–391. doi:10.1007/BF01190841.

de Bruyne, M., Clyne, P., & Carlson, J. (1999). Odor coding in a model olfactory organ: the *Drosophila* Maxillary Palp. *The Journal of Neuroscience, 19*, 4520–4532.

de Bruyne, M., Foster, K., & Carlson, J. (2001). Odor coding in the drosophila antenna. *Neuron, 30*, 537–552. doi:10.1016/S0896-6273(01)00289-6.

Destexhe, A., Bal, T., McCormick, D., & Sejnowski, T. (1996). Ionic mechanisms underlying synchronized oscillations and propagating waves in a model of ferret thalamic slices. *Journal of Neurophysiology, 76*, 2049–2070.

Duchamp-Viret, P., Duchamp, A., & Chaput, M. (2000). Peripheral odor coding in the rat and frog: quality and intensity specification. *The Journal of Neuroscience, 20*, 2383–2390.

Dutar, P., & Nicoll, R. (1988). A physiological role for GABAB Receptors in the central nervous system. *Nature, 332*, 156–158. doi:10.1038/332156a0.

Friedrich, R., & Korsching, S. (1997). Combinatorial and chemotopic odorant coding in the zebrafish olfactory bulb visualized by optical imaging. *Neuron, 18*, 737–752. doi:10.1016/S0896-6273(00)80314-1.

Friedrich, R., & Laurent, G. (2001). Dynamic optimization of odor representations by slow temporal patterning of mitral cell activity. *Science, 291*, 889–894. doi:10.1126/science.291.5505.889.

Friedrich, R., & Laurent, G. (2004). Dynamics of olfactory bulb input and output activity during odor stimulation in zebrafish. *Journal of Neurophysiology, 91*, 2658–2669. doi:10.1152/jn.01143.2003.

Fuss, S., & Korsching, S. (2001). Odorant feature detection: activity mapping of stucture response relationships in the zebrafish olfactory bulb. *The Journal of Neuroscience, 21*, 8396–8407.

Galizia, C., Sachse, S., & Mustaparta, H. (2000). Calcium responses to pheromones and plant odours in the antennal lobe of the male and female moth *Heliothis virescens*. *Journal of Comparative Physiology. A, Sensory, Neural, and Behavioral Physiology, 186*, 1049–1063. doi:10.1007/s003590000156.

Gao, Q., Yuan, B., & Chess, A. (2000). Convergent projections of drosophila olfactory neurons to specific glomeruli in the antennal lobe. *Nature Neuroscience, 3*, 780–785. doi:10.1038/75753.

Graziadei, P., & Metcalf, J. (1971). Autoradiographic and ultrastructural observations on the frog's olfactory mucosa. *Z Zellforsch Mikrosk Anat., 116*, 305–318. doi:10.1007/BF00330630.

Hallem, E., & Carlson, J. (2006). Coding of odors by a receptor repertoire. *Cell, 125*, 143–160. doi:10.1016/j.cell.2006.01.050.

Hansson, B., & Anton, S. (2000). Function and morphology of the antennal lobe: new developments. *Annual Review of Entomology, 45*, 203–231. doi:10.1146/annurev.ento.45.1.203.

Heisenberg, M. (1998). What do the mushroom bodies do for the insect brain? An Introduction. *Learning & Memory (Cold Spring Harbor, N.Y.), 5*, 1–10.

Hildebrand, J., & Shepherd, G. (1997). Mechanisms of olfactory discrimination : converging evidence for common principles across phyla. *Annual Review of Neuroscience, 20*, 595–631. doi:10.1146/annurev.neuro.20.1.595.

Hildebrand, J., Rossler, W., & Tolbert, L. (1997). Postembryonic development of the olfactory system in the moth manduca sexta: primary-afferent control of glomerular development. *Seminars in Cell & Developmental Biology, 8*, 163–170. doi:10.1006/scdb.1996.0139.

Hodgkin, A., & Huxley, A. (1952). A quantitative description of membrane current and its application to conduction and excitation in nerve. *The Journal of Physiology, 117*, 500–544.

Homberg, U., Christensen, T., & Hildebrand, J. (1989). Structure and function of the deutocerebrum in insects. *Annual Review of Entomology, 34*, 477–501. doi:10.1146/annurev.en.34.010189.002401.

Huguenard, J., Coulter, D., & McCormick, D. (1991). A fast transient potassium current in thalamic relay neurons. Kinetics of Activation and Inactivation. *Journal of Neurophysiology, 66*, 1305–1315.

Joerges, J., Küttner, A., Galizia, G., & Menzel, R. (1997). Representations of odours and odour mixtures visualized in the honeybee brain. *Nature, 387*, 285–288. doi:10.1038/387285a0.

Johnson, B., & Leon, M. (2000). Modular representation of odorants in the glomerular layer of the rat olfactory bulb and the effects of stimulus concentration. *The Journal of Comparative Neurology, 422*, 496–509. doi:10.1002/1096-9861(20000710)422:4<496::AID-CNE2>3.0.CO;2-4.

Kenyon, F. (1896). The brain of the bee. A preliminary contribution to the morphology of the nervous system of the arthropoda. *The Journal of Comparative Neurology, 6*, 133–210. doi:10.1002/cne.910060302.

Laurent, G. (1996). Dynamical representation of odors by oscillating and evolving neural assemblies. *Trends in Neurosciences, 19*, 489–496. doi:10.1016/S0166-2236(96)10054-0.

Laurent, G., & Davidowitz, H. (1994). Encoding of olfactory information with oscillating neural assemblies. *Science, 265*, 1872–1875. doi:10.1126/science.265.5180.1872.

Laurent, G., & Naraghi, M. (1994). Odorant-induced oscillations in the mushroom bodies of the locust. *The Journal of Neuroscience, 14*, 2993–3004.

Laurent, G., Seymour-Laurent, K., & Johnson, K. (1993). Dendritic excitability and a voltage-gated calcium current in locust nonspiking local interneurons. *Journal of Neurophysiology, 69*, 1484–1498.

Laurent, G., Wehr, M., & Davidowitz, H. (1996). Temporal representations of odors in an olfactory network. *The Journal of Neuroscience, 16*, 3837–3847.

Laurent, G., Stopfer, M., Friedrich, R., Rabinovich, M., Volkovskii, A., & Abarbanel, H. (2001). Odor encoding as an active, dynamical process : experiments, computation, and theory. *Annual Review of Neuroscience, 24*, 263–297. doi:10.1146/annurev.neuro.24.1.263.

Leitch, B., & Laurent, G. (1996). GABAergic synapses in the antennal lobe and mushroom body of the locust olfactory system. *The Journal of Comparative Neurology, 372*, 487–514. doi:10.1002/(SICI)1096-9861(19960902)372:4<487::AID-CNE1>3.0.CO;2-0.

MacLeod, K., & Laurent, G. (1996). Distinct mechanisms for synchronization and temporal patterning of odor-encoding neural assemblies. *Science, 274*, 976–979. doi:10.1126/science.274.5289.976.

MacLeod, K., Bäcker, A., & Laurent, G. (1998). Who reads temporal information contained across synchronized and oscillatory spike trains? *Nature, 395*, 693–698. doi:10.1038/27201.

Malnic, B., Hirono, J., Sato, T., & Buck, L. (1999). Combinatorial receptor codes for odors. *Cell, 96*, 713–723. doi:10.1016/S0092-8674(00)80581-4.

Mazor, O., & Laurent, G. (2005). Transient dynamics versus fixed points in odor representations by locust antennal lobe projection neurons. *Neuron, 48*, 661–673. doi:10.1016/j.neuron.2005.09.032.

Meister, M., & Bonhoeffer, T. (2001). Tuning and topography in an odor map on the rat olfactory bulb. *The Journal of Neuroscience, 21*, 1351–1360.

Mercer, A., & Hildebrand, J. (2002a). Developmental changes in the density of ionic currents in antennal-lobe neurons of the sphinx moth, Manduca Sexta. *Journal of Neurophysiology, 87*, 2664–2675.

Mercer, A., & Hildebrand, J. (2002b). Developmental changes in the electrophysiological properties and response characteristics of manduca antennal-lobe neurons. *Journal of Neurophysiology, 87*, 2650–2663.

Moulton, D. (1974). Dynamics of cell populations in the olfactory epithelium. *Annals of the New York Academy of Sciences, 237*, 52–61. doi:10.1111/j.1749-6632.1974.tb49843.x.

Ng, M., Roorda, R., Lima, S., Zemelman, B., Morcillo, P., & Miesenbock, G. (2002). Transmission of olfactory information between three populations of neurons in the antennal lobe of the fly. *Neuron, 36*, 463–474. doi:10.1016/S0896-6273(02)00975-3.

Perez-Orive, J., Mazor, O., Turner, G., Cassenaer, S., Wilson, R., & Laurent, G. (2002). Oscillations and sparsening of odor representations in the mushroom body. *Science, 297*, 359–365. doi:10.1126/science.1070502.

Perez-Orive, J., Bazhenov, M., & Laurent, G. (2004). Intrinsic and circuit properties favor coincidence detection for decoding oscillatory input. *The Journal of Neuroscience, 24*, 6037–6047. doi:10.1523/JNEUROSCI.1084-04.2004.

Reisenman, C., Christensen, T., Francke, W., & Hildebrand, J. (2004). Enantioselectivity of projection neurons innervating identified olfactory glomeruli. *The Journal of Neuroscience, 24*, 2602–2611. doi:10.1523/JNEUROSCI.5192-03.2004.

Rubin, B., & Katz, L. (1999). Optical imaging of odorant representations in the mammalian olfactory bulb. *Neuron, 23*, 499–511. doi:10.1016/S0896-6273(00)80803-X.

Sachse, S., & Galizia, C. (2002). Role of inhibition for temporal and spatial odor representation in olfactory output neurons: a calcium imaging study. *Journal of Neurophysiology, 87*, 1106–1117.

Sachse, S., Rappert, A., & Galizia, C. (1999). The spatial representation of chemical structures in the antennal lobes of honeybees: steps towards the olfactory code. *The European Journal of Neuroscience, 11*, 3970–3982. doi:10.1046/j.1460-9568.1999.00826.x.

Sivan, E., & Kopell, N. (2004). Mechanism and circuitry for clustering and fine discrimination of odors in insects. *Proceedings of the National Academy of Sciences of the United States of America, 101*, 17861–17866. doi:10.1073/pnas.0407858101.

Sivan, E., & Kopell, N. (2006). Oscillations and Slow Patterning in the Antennal Lobe. *Journal of Computational Neuroscience, 20*, 85–96. doi:10.1007/s10827-006-4087-z.

Sloper, J., & Powell, T. (1978). Ultrastructural features of the sensorimotor cortex of the primate. *Philosophical Transactions of the Royal Society of London. Series B, Biological Sciences, 285*, 124–139.

Stopfer, M., Bhagavan, S., Smith, B., & Laurent, G. (1997). Impaired odour discrimination on desynchronization of odour-encoding neural assemblies. *Nature, 390*, 70–74. doi:10.1038/36335.

Strausfeld, N., Hansen, L., Li, Y., Gomez, R., & Ito, K. (1998). Evolution, discovery, and interpretations of arthropod mushroom bodies. *Learning & Memory (Cold Spring Harbor, N.Y.), 5*, 11–37.

Treloar, H., Feinstein, P., Mombaerts, P., & Greer, C. (2002). Specificity of glomerular targeting by olfactory sensory axons. *The Journal of Neuroscience, 22*, 2469–2477.

Vickers, N., & Christensen, T. (1998). A combinatorial model of odor discrimination using a small array of contiguous, chemically defined glomeruli. *Annals of the New York Academy of Sciences, 855*, 514–516. doi:10.1111/j.1749-6632.1998.tb10617.x.

Vickers, N., Christensen, T., & Hildebrand, J. (1998). Combinatorial odor discrimination in the brain: attractive and antagonistic odor blends are represented in distinct combinations of uniquely identifiable glomeruli. *The Journal of Comparative Neurology, 400*, 35–36. doi:10.1002/(SICI)1096-9861(19981012)400:1<35::AID-CNE3>3.0.CO;2-U.

Vosshall, L., Wong, A., & Axel, R. (2000). An olfactory sensory map in the fly brain. *Cell, 102*, 147–159. doi:10.1016/S0092-8674(00)00021-0.

Wachowiak, M., & Cohen, L. (2001). Representation of odorants by receptor neuron input to the mouse olfactory bulb. *Neuron, 32*, 723–735. doi:10.1016/S0896-6273(01)00506-2.

Wang, J., Wong, A., Flores, J., Vosshall, L., & Axel, R. (2003). Two-photon calcium imaging reveals an odor-evoked map of activity in the fly brain. *Cell, 112*, 271–282. doi:10.1016/S0092-8674(03)00004-7.

Wehr, M., & Laurent, G. (1999). Relationship between afferent and central temporal patterns in the locust olfactory system. *The Journal of Neuroscience, 19*, 381–390.

Wilson, R., & Mainen, Z. (2006). Early events in olfactory processing. *Annual Review of Neuroscience, 29*, 163–201. doi:10.1146/annurev.neuro.29.051605.112950.

Methods

The model network consisted of 90 PNs and 30 LNs, in accordance with the experimentally observed ratio of approximately three PNs to one LN in the locust AL (Leitch and Laurent, 1996). The membrane potential of each PN and LN was governed by a single-compartment equation obeying Hodgkin-Huxley type kinetics. The PN and LN currents were taken from those used by Bazhenov *et al.* (2001) in their locust AL model.

Intrinsic Currents

Each PN was equipped with Hodgkin-Huxley sodium and potassium spiking currents as well as a transient potassium current. LNs in the locust AL, however, do not generate traditional action potentials; rather, LNs exhibit slow 20-30 ms calcium spikes that decrease in frequency after 100-200 ms of steady stimulation (Laurent *et al.*, 1993). Thus, LNs in our model network were equipped with a calcium current, a calcium-dependent potassium current, and a traditional potassium current. Details are given in the appendix.

Synaptic Currents

PN cholinergic synapses and LN GABAergic synapses were modeled by fast-activating synaptic currents. While cholinergic transmission was modeled via stereotyped neurotransmitter release in response to a presynaptic PN action potential, a continuous coupling model was used to simulate GABAergic transmission - neurotransmitter release was dependent upon the level of presynaptic LN depolarization (Laurent *et al.*, 1993). Additionally, a slow inhibitory synaptic current from LNs to PNs was introduced in order to reproduce the slow temporal patterns observed experimentally in PN odor responses (Laurent *et al.*, 1996). The current was modeled as acting through slowly-activating inhibitory receptors and required a series of approximately three LN calcium spikes to become active. A slow synaptic inhibitory current is consistent with the experimental results of Barbara *et al.* (2005) in the honeybee AL (see Discussion for further justification). Details are given in the appendix.

Network Properties

The network consisted of randomly interconnected PNs and LNs with cell-type specific connection probabilities. The PN-PN and PN-LN connection probability was 0.1, while the LN-LN connection probability was 0.25 and the LN-PN connection probability was 0.15. The lack of anatomical or functional glomerular units containing more than one PN within the locust AL suggests that spatially uniform connectivity statistics are a reasonable assumption (Leitch and Laurent, 1996; Laurent, 1996; Wilson and Mainen, 2006). We experimented with a wide range of connection probabilities and determined that sparse network connectivity (specifically sparse PN-PN connectivity) was required in order to reproduce the known features of locust AL physiology. Each PN received background current input in the form of a Poisson spike train with a mean rate of 3500 spikes/second and a spike strength of 0.0654 μA. In agreement with experiment, this resulted in a background PN firing rate of approximately 2-4 spikes/second (Perez-Orive *et al.*, 2002). All simulations were performed using the explicit Euler method with a time step of 0.01 ms.

Odor Simulation

An odor was simulated by stimulating a set of 36 PNs and 12 LNs. Each stimulated cell received stimulus current in the form of 200 independent Poisson spike trains, each with a mean rate of 35 spikes/second and a spike strength of 0.01743 μA (PNs) or 0.01667 μA (LNs). Due to the large convergence ratio of ORN inputs onto PNs in the locust (Hildebrand *et al.*, 1997; Homberg *et al.*, 1989; Mazor and Laurent, 2005) and their mean-driven log-linear response properties (Rubin and Katz, 1999; Duchamp-Viret *et al.*, 2000; Wachowiak and Cohen, 2001; Meister and Bonhoeffer, 2001; Reisenman *et al.*, 2004; Hallem and Carlson, 2006), we modeled ORN input to each AL neuron as a stochastic process (with Poisson statistics) rather than simulating individual ORNs explicitly. Consistent with experiment, PNs which were active during stimulus presentation exhibited firing rates of 10-40 spikes/second (Perez-Orive *et al.*, 2002). Twenty trials were performed for each stimulus with a 10 second total duration for each

trial. Stimulus onset occurred at $t_o = 1$ second and stimulus offset occurred at $t_d = 3.5$ seconds. In order to capture the experimentally observed time course of ORN input to the locust antennal lobe (Wehr and Laurent, 1999), we modeled stimulus rise as exponential with a rise time of 400 ms, while stimulus decay was modeled as root exponential with a decay time of approximately 1000 ms. The odor-evoked input rate of ORN spikes to a stimulated cell in the network was given by $R(t) = r_m exp(-(t - (t_o + s))^2/c_1)$ for $t = t_o$ to $t = t_o + s$, by $R(t) = r_m$ for $t = t_o + s$ to $t = t_d$, and $R(t) = r_m exp(-sqrt(t - t_d)/c_2)$ for $t > t_d$, where $s = 400$ ms was the rise time, $c_1 = 100,000$, $c_2 = sqrt(1000)$ were the scaling constants, and r_m was the maximal stimulus-evoked ORN input rate (described above).

It is generally thought that the olfactory system initially encodes odors in a combinatorial manner - different odors are represented by differing (but potentially overlapping) subsets of active ORNs (Joerges *et al.*, 1997; Vickers and Christensen, 1998; Vickers *et al.*, 1998; Malnic *et al.*, 1999; Ache and Young, 2005; Wang *et al.*, 2003; Ng *et al.*, 2002). We therefore explored one paradigm of odor simulation, referred to as the combinatorial paradigm, in which different odors were simulated by stimulating varying subsets of 36 PNs and 12 LNs, with the statistics of current input (described above) uniform across stimulated cells. In addition to coding stimuli in the combinatorial paradigm, we also examined network behavior when differing stimuli were represented via an intensity paradigm. In this case, odors were represented as intensity distributions, and the set of 36 PNs and 12 LNs receiving stimulus current was fixed across stimuli. This fixed subset of cells was divided into six groups of 6 PNs and 2 LNs, and each group was assigned a factor of 1.0, 0.9, 0.8, 0.7, 0.6, or 0.5 (with each group being assigned a distinct factor). The mean stimulus input rate to each group was multiplied by its assigned factor (with otherwise unaltered current input statistics), and different odors were simulated by rearranging the group-factor assignments. The intensity paradigm of odor encoding was motivated by the observation that varying the concentration of a given odor tends to modulate the firing rates of responding ORNs in vivo (de Bruyne *et al.*, 2001; Wang *et al.*, 2003; Friedrich and Korsching, 1997; Meister and Bonhoeffer, 2001), and hence stimuli coded in the intensity paradigm can be thought of as representing differing concentrations of the same odor.

Local Field Potential

In the locust, the local field potential (LFP) is measured from the mushroom body, and oscillations in the LFP are taken as an indicator of PN synchrony (Laurent *et al.*, 1996). In order to assess PN synchrony in our model, we computed the LFP of the network as the average membrane potential of all 90 PNs. The power spectrum of the LFP of the PN odor response was computed during the period of stimulus presentation (1-3.5 sec) using a single trial. Additionally, we computed the total integrated power of the LFP in the 15-25 Hz range as a function of time; the integrated power was computed in 200 ms sliding windows with a 50 ms step size and was averaged over the 20 trials performed for a given stimulus.

Principal Component Analysis

Principal component analysis (PCA) was performed on the stimulus-response data of the network. For a given stimulus, we computed the 90×2000 matrix of PN firing rates in 50 ms time bins over the entire 10 second trial duration; the matrix entries were then averaged over the 20 trials performed for the given stimulus. We performed PCA on the matrix of trial-averaged PN firing rates, projected the data onto the first three principal components, and plotted the resulting three dimensional stimulus-response trajectories. By dividing the sum of the magnitudes of the eigenvalues of the first three principal components by the sum of the magnitudes of all eigenvalues, we computed the fraction of the data variance captured by the first three principal components. In all cases, the first three principal components captured more than 90% of the total data variance. Stimulus-response trajectories resulting from single trial data matrices were similar to trial-averaged trajectories; however, trial-averaged trajectories were more well-defined and thus these are shown in plots. Qualitatively, the general features exhibited by the dynamics of the response trajectory were independent of the stimulus used.

Odor Discrimination

We used a simple algorithm based on distances of individual trial firing rate vectors to template firing rate vectors for each odor to assess stimulus classification by the model network. To test the ability of the network to discriminate among N simulated odors in a given 50 ms time bin, we computed the 90 dimensional vector of trial-averaged PN firing rates for each of the N odors in the 50 ms bin; these vectors were used as the templates for each of the N odors. For each of the 20N trials, we computed the Euclidean distance between the vector of PN firing rates for the trial and each of the odor templates. If the Euclidean distance from the trial to each of the odor templates was minimized for odor j, we designated that the network classified the trial as a presentation of odor j. If the trial was indeed a presentation of odor j, then the trial was deemed correctly classified by the network, and the discriminability of the network in the given 50 ms time bin was determined as the fraction of the 20N trials correctly classified by the network. The overall ability of the network to discriminate among the N simulated odors was determined as the time-averaged discriminability of the network during the period of stimulus presentation (1-3.5 seconds).

We chose this particular linear discriminator to match that utilized by Mazor and Laurent (2005) in their analysis of odor discrimination using stimulus-evoked recordings from locust PNs. The choice of 50 ms time bins was motivated by the physiology of Kenyon cells (KCs), the neurons of the mushroom body that read PN activity (Kenyon, 1896; Laurent and Naraghi, 1994). PNs send barrages of spikes to both KCs and LHIs, which are GABAergic interneurons located in a structure called the lateral horn (Hansson and Anton, 2000). Additionally, 20 Hz oscillations seen in the LFP of the mushroom body indicate that PN input to KCs and LHIs is globally synchronized on a 50 ms time scale (Laurent and Davidowitz, 1994; Laurent *et al.*, 1996). Since KC dendrites are known to receive GABAergic input (Leitch and Laurent, 1996) and LHI axon collaterals have been shown to diffusely overlap KC dendrites, LHIs are the likely source of the strong, periodic, phase-delayed inhibition seen in recordings from KCs (Perez-Orive *et al.*, 2002). Thus, KCs receive globally synchronized PN input in 50 ms epochs, and towards the end of each epoch the membrane potential of every KC is effectively reset by inhibition arriving from the lateral horn. This suggests that KCs integrate PN activity over a time scale no greater than 50 ms, and hence it is probable that odor discrimination in the locust brain occurs over similar temporal windows.

Appendix

The membrane potential of each PN and each LN was governed by equations of the following form:

$$C_m \frac{dV_{PN}}{dt} = -g_L(V_{PN} - E_L) - I_{Na} - I_K - I_A$$
$$-I_{GABA} - I_{slow} - I_{nACH} - I_{stim}$$
$$C_m \frac{dV_{LN}}{dt} = -g_L(V_{LN} - E_L) - I_{Ca} - I_{CaK} - I_K$$
$$-I_{GABA} - I_{nACH} - I_{stim}.$$

The parameters for the passive leak current were $C_m = 1.0\ \mu F$, $g_L = 0.3\ \mu S$, $E_L = -64\ mV$ for PNs and $C_m = 1.0\ \mu F$, $g_L = 0.3\ \mu S$, $E_L = -50\ mV$ for LNs.

Intrinsic Currents

The intrinsic currents consisted of fast sodium and potassium currents I_{Na} and I_K, a transient calcium current I_{Ca}, a calcium-dependent potassium current I_{CaK}, and a transient potassium current I_A. All such currents obeyed equations of the following form:

$$I_j = g_j m^M h^N (V - E_j).$$

The maximal conductances were $g_{Na} = 120\ \mu S$, $g_K = 3.6\ \mu S$, $g_A = 1.43\ \mu S$ for PNs and $g_{Ca} = 5.0\ \mu S$, $g_{CaK} = 0.045\ \mu S$, $g_K = 36\ \mu S$ for LNs. The reversal potentials were $E_{Na} = 40\ mV$, $E_K = -87\ mV$ for PNs and $E_{Ca} = 140\ mV$, $E_K = -95\ mV$ for LNs.

The gating variables $m(t)$ and $h(t)$ take values between 0 and 1 and obey the following equations:

$$\frac{dm}{dt} = \frac{m_\infty(V) - m}{\tau_m(V)}$$

$$\frac{dh}{dt} = \frac{h_\infty(V) - h}{\tau_h(V)}.$$

I_{Na} and I_K are described in Hodgkin and Huxley (1952).

The I_{Ca} current has $M = 2$, $N = 1$, $m_\infty = 1/(1 + exp(-(V + 20)/6.5))$, $\tau_m = 1 + (V + 30)0.014$, $h_\infty = 1/(1 + exp((V + 25)/12))$, $\tau_h = 0.3exp((V - 40)/13) + 0.002exp(-(V - 60)/29)$ (Laurent *et al.*, 1993).

The I_{CaK} current has $M = 1$, $N = 0$, $m_\infty = [Ca]/([Ca] + 2)$, $\tau_m = 100/([Ca] + 2)$ (Sloper and Powell, 1978).

The I_A current has $M = 4$, $N = 1$, $m_\infty = 1/(1 + exp(-(V + 60)/8.5))$, $\tau_m = (0.27/(exp((V + 35.8)/19.7) + exp(-(V + 79.7)/12.7)) + 0.1)$, $h_\infty = 1/(1 + exp((V + 78)/6))$, $\tau_h = 0.27/(exp((V + 46)/5) + exp(-(V + 238)/37.5))$ for $V < -63\ mV$ and $\tau_h = 5.1$ for $V > -63\ mV$ (Huguenard *et al.*, 1991).

The dynamics of intracellular calcium concentration [Ca] were governed by the following equation:

$$\frac{d[Ca]}{dt} = -AI_T - \frac{[Ca] - [Ca]_\infty}{\tau},$$

where $[Ca]_\infty = 0.00024\ mM$, $A = 0.0002\ mM \cdot cm^2/(ms \cdot \mu A)$, and $\tau = 150\ ms$.

Synaptic Currents

The GABA and nicotinic acetylcholine currents were governed by equations of the following form:

$$I_j = g_j[O](V - E_j).$$

The reversal potentials were $E_{nACH} = 0\ mV$ and $E_{GABA} = -70\ mV$. The fraction of open channels [O] obeyed the equation

$$\frac{d[O]}{dt} = \alpha(1 - [O])[T] - \beta[O].$$

For nicotinic acetylcholine synapses [T] was governed by the equation

$$[T] = A\theta(t_0 + t_{max} - t)\theta(t - t_0).$$

For GABAergic synapses [T] was governed by the equation

$$[T] = \frac{1}{1 + exp(-(V(t) - V_0)/\sigma)}.$$

$\theta(x)$ is the Heaviside step function, t_0 is the time of receptor activation, $A = 0.5$, $t_{max} = 0.3\ ms$, $V_0 = -20\ mV$, and $\sigma = 1.5$. For GABAergic synapses the rate constants were $\alpha = 10\ ms^{-1}$ and $\beta = 0.16\ ms^{-1}$, while for nicotinic acetylcholine synapses the rate constants were $\alpha = 10\ ms^{-1}$ and $\beta = 0.2\ ms^{-1}$ (Bazhenov *et al.*, 2001).

The slow inhibitory current from LNs to PNs was governed by the following scheme:

$$I_{slow} = g_{slow}\frac{[G]^4}{[G]^4 + K}(V - E_K)$$

$$\frac{d[R]}{dt} = r_1(1 - [R])[T] - r_2[R]$$

$$\frac{d[G]}{dt} = r_3[R] - r_4[G],$$

where the reversal potential was $E_K = -95\ mV$ and the rate constants were $r_1 = 0.5\ mM^{-1}ms^{-1}$, $r_2 = 0.0013\ ms^{-1}$, $r_3 = 0.1\ ms^{-1}$, $r_4 = 0.033\ ms^{-1}$, and $K = 100\ \mu M^4$ (Destexhe *et al.*, 1996; Bazhenov *et al.*, 1998).

Maximal synaptic conductances were $g_{GABA} = 0.3\ \mu S$ from LNs to LNs, $g_{GABA} = 0.36\ \mu S$ and $g_{slow} = 0.36\ \mu S$ from LNs to PNs, $g_{nACH} = 0.045\ \mu S$ from PNs to LNs, and $g_{nACH} = 0.009\ \mu S$ from PNs to PNs.